Applied Physics Letters ARTICLE scitation.org/journal/apl

Weight adjustable photonic synapse by nonlinear gain in a vertical cavity semiconductor optical amplifier

Cite as: Appl. Phys. Lett. **119**, 201104 (2021); doi: 10.1063/5.0064374
Submitted: 22 July 2021 · Accepted: 26 October 2021 ·
Published Online: 17 November 2021

View Online Export Citation CrossMark

Juan Arturo Alanis, Joshua Robertson, Matěj Hejda, and Antonio Hurtado[a)]

AFFILIATIONS

Institute of Photonics, Department of Physics, University of Strathclyde, Glasgow, United Kingdom

Note: This paper is part of the APL Special Collection on Neuromorphic Computing: From Quantum Materials to Emergent Connectivity.
[a)]**Author to whom correspondence should be addressed:** antonio.hurtado@strath.ac.uk

ABSTRACT

In this paper, we report a high-speed and tunable photonic synaptic element based on a vertical cavity semiconductor optical amplifier (VCSOA) operating with short (150 ps-long) and low-energy (μW peak power) light pulses. By exploiting nonlinear gain properties of VCSOAs when subject to external optical injection, our system permits full weight tunability of sub-ns input light pulses, just by varying the VCSOA's applied bias current. Not only is the VCSOA-based synapse able to adjust the strength of incoming optical pulses, but it can also provide gain (applied weight factors >1). Moreover, we show that this simple approach permits dynamical weight tuning at high-speed (ns rates) with up to an 11.6-bit precision. These results are realized with commercially sourced, inexpensive vertical cavity surface emitting lasers, operating at the key telecom wavelengths of 1300 and 1550 nm and hence making our approach compatible with optical network and data center technologies. This VCSOA-based system, therefore, offers a hardware friendly, low-energy, and high-speed solution for photonic synaptic links with high potential for use in future neuromorphic photonic systems.

Recently, the widespread use of machine learning (ML) approaches has contributed to the development of artificial intelligence (AI) to perform complex human-like information processing tasks such as learning, computer vision, natural language processing, and complex pattern recognition.[1] Current state-of-the-art neuromorphic (brain-like) computing systems realize hardware electronic neural networks based on conventional CMOS technology.[2,3] With the size of transistors reaching its physical limit,[4] more complex neural networks come at the expense of a large device footprint and energy consumption. As an alternative to the CMOS-based paradigm, photonic systems have been raising interest in recent years.[5,6] In particular, vertical-cavity surface-emitting lasers (VCSELs) are emerging as candidates for artificial neurons or nodes in photonic neural networks (PNNs). These devices exhibit many of the key neuronal characteristics, e.g., inter-connectivity, fast sub-ns spiking operation, and thresholding, which has led to applications for spiking photonic VCSEL neurons in recent years[7–9] and on chip fully connected arrays for PNNs.[10] Additionally, the use of VCSELs for photonic reservoir computing (RC) has also been recently demonstrated.[11–13]

One key aspect of neuromorphic systems is the ability to perform synaptic weighting operations of signals propagating between nodes [Fig. 1(a)]. In recent years, photonic synapses have been experimentally demonstrated either photoelectrically with the use of memristive devices[14] or in photonic integrated circuits via phase change materials.[15] The use of VCSELs for synaptic control via spike timing dependent plasticity (STDP) has been theorized.[16,17] Thus, having been used as artificial spiking neurons with fast-speed and low-energy operation (sub-nanosecond rates, <pJ/spike), VCSELs are also suitable candidates for use as photonic synapses toward energy efficient and low-footprint neuromorphic systems.

Here, we demonstrate the experimental realization of a photonic synaptic element with a VCSEL. Our approach exploits the nonlinear gain in VCSELs, when operated below their lasing threshold, as vertical-cavity semiconductor optical amplifiers (VCSOAs).[18] The VCSOA-based synapse can operate with fast 150 ps-long input optical pulses (spikes) and perform high-speed weight tunability at 0.5 GHz with values limited only by our experimental setup's capabilities. Moreover, the VCSOA-based synapse operates with low input power

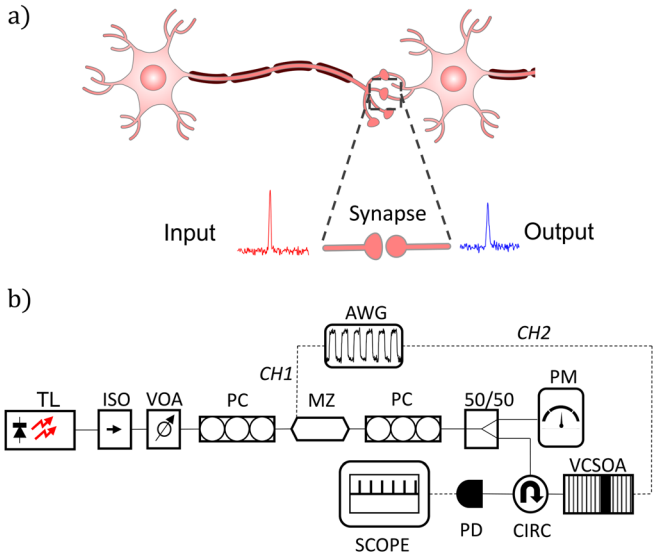

FIG. 1. (a) Illustration depicting the synaptic connection between two neurons, where the strength of an input signal (red) is weighted (blue). (b) Schematic description of the experimental setup used to demonstrate the photonic VCSOA-based synapse consisting of a tunable laser (TL), an optical isolator (ISO), a variable optical attenuator (VOA), a polarization controller (PC), a Mach–Zehnder modulator (MZM), a two-channel arbitrary waveform generator (AWG), a power meter (PM), a 50/50 splitter, an optical circulator (CIRC), a photodetector (PD), and an oscilloscope (SCOPE). Continuous and dashed lines indicate fiber-optic and electronic connections, respectively. The AWG channel one (CH1) is connected to the MZ, whereas channel 2 (CH2) modulates the VCSOA's bias current.

signals, down to tens of μWs (and possibly lower) and requiring only μA of current for dynamical weight control. Additionally, good weight resolution is demonstrated with the VCSOA-based synapse yielding up to 11.6-bit precision values, comparable to alternative photonic synapses realizations with microring resonators[19] or phase change materials.[20] Furthermore, our VCSOA-based synapse provides amplification, offering prospects for high fan-out platforms for networked systems. In addition, our approach uses off-the-shelf VCSELs and fiber-optic components at key telecom wavelengths (1300 and 1550 nm), making our approach compatible with optical communication networks.

An all-fiber-optic system was used to inject light from a tunable laser (TL) into a VCSOA [see Fig. 1(b)]. Two VCSOAs were used in this work with operation at the wavelengths of 1300 and 1550 nm, respectively. First, we used a commercially sourced (RayCan), single-mode, 1300 nm, VCSEL, operating below its threshold current ($I_{th} = 2.389$ mA at $T = 293$ K) with a dominant (parallel-polarized) resonant mode at $\lambda_{VCSOA} \simeq 1306$ nm (measured at threshold). Throughout the experiments, the VCSOA was biased below threshold with a current value $<95\% I_{th}$, and the temperature was stabilized at 293 K to ensure operation in the nonlinear gain region.[18] The TL's output is coupled to an optical isolator (ISO) to avoid spurious reflections, and its optical power is controlled with a variable optical attenuator (VOA). Using a polarization controller (PC), the TL's light is polarization matched to a Mach–Zehnder modulator (MZM). The resulting modulated signal is injected into the VCSOA's parallel-polarized mode [via an optical circulator (CIRC)] with a small negative frequency detuning ($\Delta f \approx -2.81$ GHz at a bias $I_{DC} = 0.93 * I_{th}$). This is illustrated graphically in Fig. 2 left column ("wavelength detuning"), where blue and red curves correspond to the VCSOA and TL's optical spectra, respectively. The TL's light was modulated with the MZM using channel 1 (CH1) of a 2-channel 12 GSa/s arbitrary waveform generator (AWG) to generate ~150 ps-long pulses (limited by the maximum sample rate of the AWG) with a repetition rate of 31 MHz and an average peak optical intensity of 44.5 ± 1.4 μW, as shown in the mid-column plots of Fig. 2 ("input pulse"). The modulated optical signal was then polarization-matched to the VCSOA's parallel-polarized mode by a PC and divided by a 50/50 splitter. The first branch was connected to a power meter (PM) to monitor the input power, while the second one was connected to an optical circulator (CIRC) for its injection into the VCSOA. The VCSOA's output was collected from the CIRC, detected with a fast (>9 GHz) amplified photodetector (PD) and analyzed using a fast (8 GHz) real-time oscilloscope (SCOPE). During the experiments, we controlled the VCSOA's current to tune the weights applied to the input optical pulses. First, we varied the DC bias current to perform static weight control. Later, we performed dynamical weight control at a rate of 500 MHz by modulating the VCSOA's current using channel 2 (CH2) of the AWG and a bias-tee (with 500 MHz maximum frequency) connected to the device.

Figure 2 illustrates the system's operation for three different values of the bias current applied to the VCSOA, namely, 2.245 [Fig. 2(a)], 2.210 [Fig. 2(b)], and 2.179 mA [Fig. 2(c)]. The plots shown in the left-most wavelength detuning column depict (in red) optical spectra of the injected TL signal (which is the same for the three cases) and the free-running VCSOA (in blue) measured at three different current values. As the current is gradually reduced, the VCSOA's resonant wavelength shifts away from the external injection and the initial frequency detuning (between the VCSOA and external signal) grows from -2.8 GHz [$I_{DC} = 2.245$ mA, Fig. 2(a)] to -5.6 GHz [$I_{DC} = 2.21$ mA, Fig. 2(b)] and -9.3 GHz [$I_{DC} = 2.179$ mA, Fig. 2(c)]. The plots in the "input pulse" and "weighted output" columns show the measured time series at the input and output of the VCSOA, respectively, associated with each of the three bias currents. For the set bias current of 2.245 mA, the detuning between the TL and the VCSOA is equal to -2.81 GHz. In this situation, the VCSOA's parallel mode is injection-locked to the external signal. Hence, the response from the VCSOA is maximized, producing an amplified optical pulse reaching a peak intensity of 75.9 μW. This corresponds to a weighting factor of 1.79, where the output pulse is stronger than the injected one, therefore effectively achieving gain. In the case of Fig. 2(b), where a smaller bias current of 2.21 mA is used, for the same optical input pulse (middle plot), the VCSOA outputs result in a 36.9 μW peak pulse corresponding to a weight factor of 0.77. This is due to the decreased coupling between the TL and VCSOA, as the frequency detuning between the external injection and the VCSOA's parallel-mode is increased to -5.6 GHz. Finally, Fig. 2(c) shows the response when the bias current is $I_{DC} = 2.179$ mA. In this third case, the relatively large frequency detuning of -9.32 GHz yields a highly reduced coupling between external injection and VCSOAs, resulting in a low amplitude output pulse with a 10 μW peak optical power in response to the same input pulse.

Figure 2(d) plots the VCSOA's average peak power in response to the 150 ps-long input optical pulses, where the red dashed lines

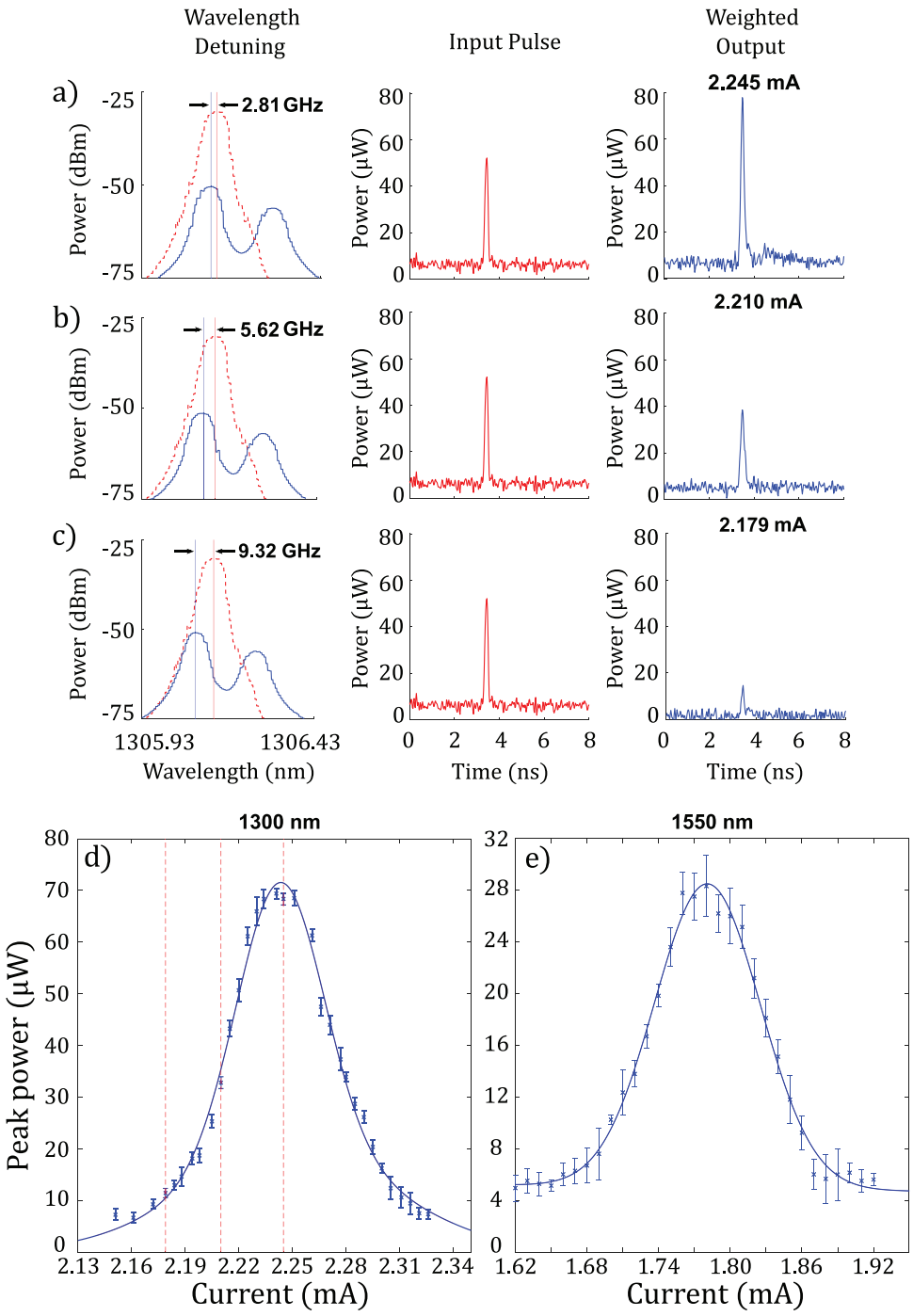

FIG. 2. Measured optical spectra of the TL's emission (red) and the free-running VCSOA (blue) associated with (a) low (−2.81 GHz), (b) moderate (−5.62 GHz), and (c) high (−9.32 GHz) frequency detuning (wavelength detuning column). The plots in the middle (input pulse) column show an example of the 150 ps-long input optical pulse of 44.5 μW peak power used in all cases. The last (weighted output) column plots show the VCSOA's measured output pulses. (d) Optical pulse peak power measured at the output of the 1300 nm-VCSOA vs applied bias current. Each point in the plot represents the mean optical pulse peak value for a sample size $n = 6$, and the error bars indicate one standard deviation. The red vertical lines highlight the three individual cases, shown in (a)–(c). (e) Average optical pulse peak power measured at the output of the 1550 nm-VCSOA vs the applied bias current, where the sample size $n = 6$ and the error bars indicate one standard deviation.

indicate the data shown in Figs. 2(a)–2(c). Specifically, Fig. 2(d) shows the mean peak amplitude of the optical pulses at the VCSOA's output (sample size $n = 6$) vs the device's bias current, where a Gaussian function is used to fit the nonlinear trajectory. A maximum average pulse peak power of ~70 μW is measured for the current of 2.245 mA. For that operation point, the system is configured to yield maximized output, by setting the wavelengths of the externally injected signal and the VCSOA's parallel-polarized mode in resonance. This yields full coupling between the external light signal and the VCSOA, resulting in the maximum output pulse peak power. Reducing (or increasing) the VCSOA's bias current from the optimum value gradually shifts the VCSOA's wavelength away from that of the externally injected signal,

bringing both signals off resonance leading to a gradual decrease in the amplitude of the measured optical pulses at the VCSOA's output. This indicates that the 1300 nm-VCSOA has a dynamic range (i.e., the range divided by the maximum error) of 21.3 dB, meaning it can reliably weight input pulses with a 11.6-bit precision. These values are comparable with other reported photonic synapses based on microring resonators[19] and phase change materials.[20] Similarly, in Fig. 2(e), we show the average peak power vs the applied current using a commercial (RayCan), single-mode, 1550 nm-VCSEL biased below threshold ($I_{th} = 1.86$ mA at $T = 293$ K). For this experiment, a 1550 nm-TL was modulated to generate 150 ps pulses with an average peak power of $18.82 \pm 1.32\,\mu$W ($n = 6$) at a rate of 31 MHz and the wavelength matched to the VCSOA's parallel-polarized mode at 95%I_{th}. At resonance, we measure a maximum pulse peak power of 28.32 μW for a set current of 1.76 mA, corresponding to a weight factor of 1.57. Analogous to the 1300 nm VCSOA, the amplitude of the output pulses in the 1550 nm-VCSOA is reduced by decreasing (or increasing) the bias current. We note that the spread in the output peak power is larger for the 1550 nm VCSOA due to the lower power (~18 μW) input pulses. However, Fig. 2(e) still reveals an achieved dynamic range of 13 dB or 4.9-bit precision with larger spreads in average output power expected for increasing input pulse amplitudes.

Figures 2(d) and 2(e), thus, clearly show the system's ability to perform synaptic weighting behavior, enabling to controllably tune the weighted optical pulse's intensity by simply using the VCSOA's bias current as the control mechanism. Moreover, the system also provides amplification as the maximum average optical pulse peak power of 70 and 28.32 μW exceeds the input pulse peak intensities of 44.5 and 18 μW, set for the 1300 and 1550 nm devices, respectively. In addition, the proposed system is able to operate with very low power (tens of μWs and possibly lower) and high-speed optical signals (150 ps-long were used due to the AWG sample rate, but operation with faster signals is possible) to deliver full weight tunability with very small variations (<0.1 mA) on the VCSOA's applied bias current. These properties highlight the low energy operation requirements of the proposed photonic synaptic system.

We further demonstrate dynamical weight control at high-speed in our proposed photonic VCSOA synapse. First, we used a commercial RayCan, single-mode, 1300 nm-VCSEL ($I_{th} = 0.77$ mA at $T = 293$ K) with a dominant parallel mode at $\lambda_{VCSOA} \simeq 1290$ nm at threshold. The VCSOA current was modulated via the second channel CH2 of the AWG using a bias-tee to introduce a 500 MHz square wave modulation signal into the device's DC bias current (limited by the bias-tee's bandwidth), which alternates the injection current between pre-set low (~0.69 mA) and high (~0.73 mA; 95%I_{th}) levels every 2 ns. This is analogous to applying two discrete weight values W_1 and W_2 [Fig. 3(b)]. In parallel, the 1300 nm-TL was modulated to produce an optical injection signal consisting of 150 ps-long pulses with an average peak power of $43.80 \pm 1.67\,\mu$W [Fig. 3(a)] and the frequency matched to the VCSOA's main resonant mode at 95%I_{th}. As a result of the current modulation, the 1300 nm-VCSOA photonic synapse is able to adjust the weights of the incoming signal at a fast rate of 0.5 GHz, yielding low and high amplitude optical pulses at the VCSOA's output [Fig. 3(c)] with average peak powers of 13.5 and 60 μW, respectively.

We also show dynamical weight control functionality at fast-speed using the 1550 nm-VCSEL, by alternating the device's injection

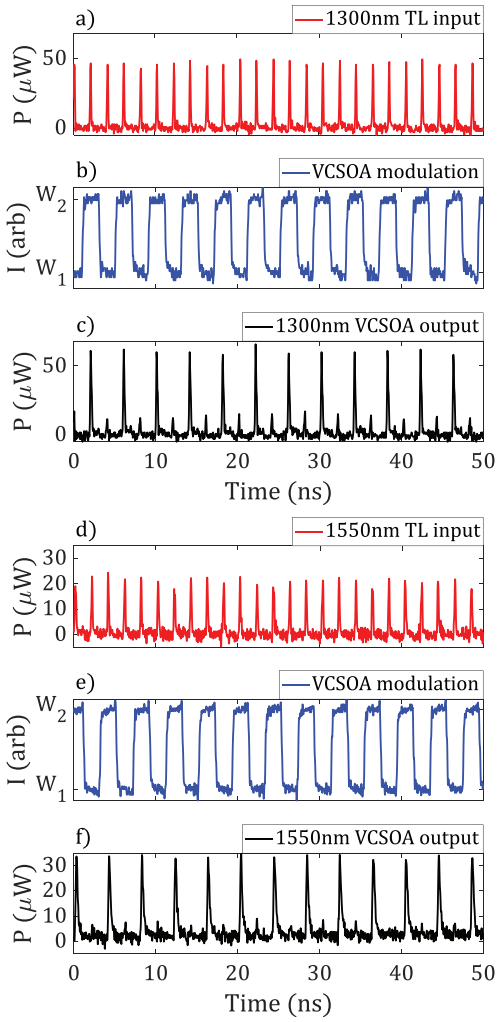

FIG. 3. (a) 1300 nm-TL optical input signal consisting of continuous 150 ps pulses repeating every 2 ns. (b) Modulation signal used to drive the VCSOA's bias current between low (0.70 mA) and high (0.73 mA) levels, analogous to applying two discrete weights values W_1 and W_2. (c) Recorded 1300 nm-VCSOA output showing dynamic weight tunability of the optical pulses yielding low and high amplitudes at high-speed. (d) 1550 nm-TL optical input signal consisting of continuous 150 ps pulses repeating every 2 ns. (e) Modulation signal used to drive the VCSOA's bias current between a low (1.71 mA) and high (1.75 mA) level. (f) Recorded VCSOA output showing weight tunability of the optical pulses for the 1550 nm device.

current between ~1.70 and ~1.75 mA (associated with W_1 and W_2) every 2 ns using a square modulation [Fig. 3(e)]. Then, we used the 1550 nm-TL and MZ to inject 150 ps pulses at the same repetition rate with an average peak power of $21.48 \pm 1.69\,\mu$W [Fig. 3(d)]. The TL peak was frequency matched to the VCSOA's parallel-polarized resonant mode at 95%I_{th}. Similarly, we measured the optical pulse amplitude at the system's output and found that the 1550 nm-VCSOA is able to dynamically adjust the intensity of the input pulses at 0.5 GHz in accordance with the pre-set W_1 and W_2 values, resulting in a low and high average peak amplitude of 7.1 and 33.6 μW, respectively. These results show the capacity of VCSOAs for high-speed dynamical

weight tunability at the 1300 and 1550 ns key telecom wavelengths. We must note that the selected 0.5 GHz frequency is the maximum rate of the used bias-tee. However, we expect the commercially sourced VCSELs of this work to operate at higher frequencies of 1 GHz, determined by their carrier recombination times of ∼1 ns. Faster rates might be possible for devices including additional design optimization stages.

Finally, we show experimental results when introducing a multi-level signal to the 1550 nm-VCSOA such that the bias current switches between five distinct levels every 2 ns (in the range of $\sim 1.70 < I \lesssim 1.75$ mA), associated with discrete weight values going from $W_1 \rightarrow W_5$ [Fig. 4(a)]. For this experiment, the 1500 nm-TL optical injection pulses were the same as in Fig. 3(d). The corresponding time-trace, measured at the output of the VCSOA, shows that the system is able to tune the pulse amplitude in accordance with the multi-level current modulation, essentially assigning five unique weights to incoming 150 ps-long pulses [Fig. 4(b)]. This is shown in Fig. 5, plotting the mean peak power for the weights applied in Fig. 4(b), revealing that the 1550 nm VCSOA-based synapse can dynamically weight input pulses with a dynamic range of 16 dB (6.3-bit precision). Moreover, the pulse amplitude can be tuned with small changes in current, requiring tens of μWs per weight value and further highlighting that the potential VCSOAs have low-energy synaptic links for photonic neuromorphic platforms.

We demonstrate experimentally a photonic synaptic system based on a telecom-wavelength, off-the-shelf VCSEL biased below threshold (operating as a VCSOA), permitting the controlled weighting (and amplification) of optical signals (short optical pulses). By controlling the device's bias current, we create an effective, low energy, and high-speed weight tuning mechanism. We show the capability to apply controllable weights to fast optical pulses (150 ps-long), achieving output peak powers ranging from near zero to amplified values

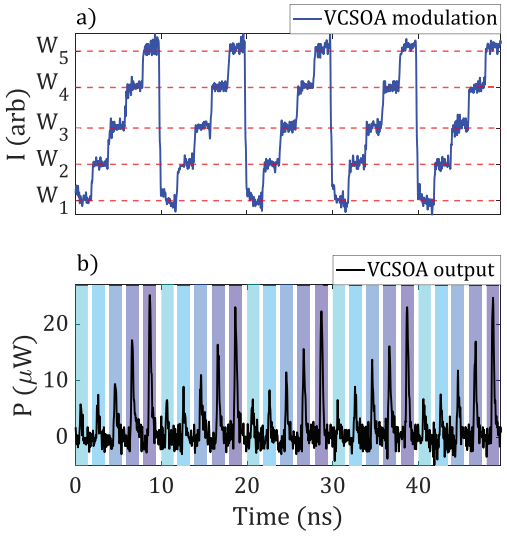

FIG. 4. (a) Five level modulation signal used to drive the 1550 nm-VCSOA's current, where each level is associated with distinct weight values going from $W_1 \rightarrow W_5$. (b) Recorded VCSOA output time-trace showing dynamical weight control of the optical pulses yielding five distinct levels with increasing amplitude.

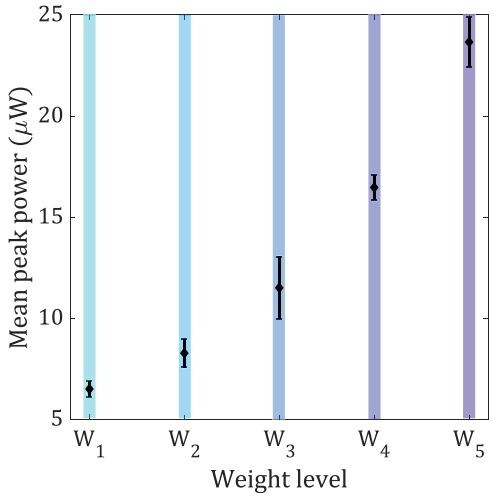

FIG. 5. Mean peak power values associated with five assigned weight levels, showing the VCSOA-based synapse is able to reliably set discrete weights to optical pulses. Each point was calculated from the output time-trace shown in Fig. 4(b).

with up to 11.6-bit precision (21.3 dB dynamic range) and permitting weight tuning via small current changes (a few μAs). Furthermore, the system operates with high-speed and low-power optical signals of tens of μWs of peak power. Thus, VCSOAs offer a potential solution toward low-energy operation of spiking PNNs, where the node density is typically outweighed by the number of synapses. Additionally, the system allows for dynamic and effective weight control by modulating the device bias current with user-defined signals. The weight control of the VCSOA-based synapse can, therefore, be adjusted either by tuning the device bias current, by introducing a current modulation signal, or a combination of both. This result demonstrates the potential of VCSELs functioning as VCSOAs as hardware-friendly photonic synaptic elements in neuromorphic platforms for future light-based artificial intelligence systems.

The authors acknowledge support from the UKRI Turing AI Acceleration Fellowship Programme (No. EP/V025198/1), the U.S. Office of Naval Research Global (Grant No. ONRG-NICOP-N62909-18-1-2027), the European Commission (Grant No. 828841-ChipAI-H2020-FETOPEN-2018-2020), and the EPSRC Doctoral Training Partnership (No. EP/N509760).

AUTHOR DECLARATIONS

Conflict of Interest

The authors have no conflicts to disclose.

DATA AVAILABILITY

The data that support the findings of this study are openly available in University of Strathclyde's KnowledgeBase at https://doi.org/10.15129/89eefc99-f1ee-4870-bbda-2d46fb57d723.

REFERENCES

[1]E. Callaway, "'It will change everything': DeepMind's AI makes gigantic leap in solving protein structures," Nature **588**, 203–204 (2020).

[2]M. Davies, N. Srinivasa, T.-H. Lin, G. Chinya, Y. Cao, S. H. Choday, G. Dimou, P. Joshi, N. Imam, S. Jain, Y. Liao, C.-K. Lin, A. Lines, R. Liu, D. Mathaikutty, S. McCoy, A. Paul, J. Tse, G. Venkataramanan, Y.-H. Weng, A. Wild, Y. Yang, and H. Wang, "Loihi: A neuromorphic manycore processor with on-chip learning," IEEE Micro **38**, 82–99 (2018).
[3]M. V. DeBole, R. Appuswamy, P. J. Carlson, A. S. Cassidy, P. Datta, S. K. Esser, G. J. Garreau, K. L. Holland, S. Lekuch, M. Mastro, J. McKinstry, B. Taba, C. di Nolfo, B. Paulovicks, J. Sawada, K. Schleupen, B. G. Shaw, J. L. Klamo, M. D. Flickner, J. V. Arthur, D. S. Modha, A. Amir, F. Akopyan, A. Andreopoulos, W. P. Risk, J. Kusnitz, C. Ortega Otero, and T. K. Nayak, "TrueNorth: Accelerating from zero to 64 million neurons in 10 years," Computer **52**, 20–29 (2019).
[4]J. Shalf, "The future of computing beyond Moore's law," Philos. Trans. R. Soc. A **378**, 20190061 (2020).
[5]L. De Marinis, M. Cococcioni, P. Castoldi, and N. Andriolli, "Photonic neural networks: A survey," IEEE Access **7**, 175827–175841 (2019).
[6]T. F. de Lima, H.-T. Peng, A. N. Tait, M. A. Nahmias, H. B. Miller, B. J. Shastri, and P. R. Prucnal, "Machine learning with neuromorphic photonics," J. Lightwave Technol. **37**, 1515–1534 (2019).
[7]J. Robertson, E. Wade, Y. Kopp, J. Bueno, and A. Hurtado, "Toward neuromorphic photonic networks of ultrafast spiking laser neurons," IEEE J. Sel. Top. Quantum Electron. **26**, 7700715 (2020).
[8]M. Hejda, J. Robertson, J. Bueno, and A. Hurtado, "Spike-based information encoding in vertical cavity surface emitting lasers for neuromorphic photonic systems," J. Phys. **2**, 044001 (2020).
[9]Y. Zhang, J. Robertson, S. Xiang, M. Hejda, J. Bueno, and A. Hurtado, "All-optical neuromorphic binary convolution with a spiking VCSEL neuron for image gradient magnitudes," Photonics Res. **9**, B201 (2021).
[10]T. Heuser, M. Pflüger, I. Fischer, J. A. Lott, D. Brunner, and S. Reitzenstein, "Developing a photonic hardware platform for brain-inspired computing based on 5×5 VCSEL arrays," J. Phys. **2**, 044002 (2020).
[11]G. Van der Sande, D. Brunner, and M. C. Soriano, "Advances in photonic reservoir computing," Nanophotonics **6**, 561–576 (2017).
[12]J. Vatin, D. Rontani, and M. Sciamanna, "Experimental reservoir computing using VCSEL polarization dynamics," Opt. Express **27**, 18579 (2019).
[13]J. Bueno, J. Robertson, M. Hejda, and A. Hurtado, "Comprehensive performance analysis of a VCSEL-based photonic reservoir computer," IEEE Photonics Technol. Lett. **33**, 920–921 (2021).
[14]A. Emboras, A. Alabastri, P. Lehmann, K. Portner, C. Weilenmann, P. Ma, B. Cheng, M. Lewerenz, E. Passerini, U. Koch, J. Aeschlimann, F. Ducry, J. Leuthold, and M. Luisier, "Opto-electronic memristors: Prospects and challenges in neuromorphic computing," Appl. Phys. Lett. **117**, 230502 (2020).
[15]J. Wang, L. Wang, and J. Liu, "Overview of phase-change materials based photonic devices," IEEE Access **8**, 121211–121245 (2020).
[16]S. Xiang, Y. Zhang, J. Gong, X. Guo, L. Lin, and Y. Hao, "STDP-based unsupervised spike pattern learning in a photonic spiking neural network with VCSELs and VCSOAs," IEEE J. Sel. Top. Quantum Electron. **25**, 1700109 (2019).
[17]T. Tian, M. Ni, Zhengmao, W. Guangqiong, X. Xiaodong, and L. Tao Deng, "Theoretical investigation of weight-dependent optical spike timing dependent plasticity based on VCSOA," J. Phys. **1792**, 012037 (2021).
[18]A. Hurtado, I. D. Henning, and M. J. Adams, "Bistability and nonlinear gain in 1.55 μm vertical cavity semiconductor optical amplifiers: Theory and experiments," Appl. Phys. Lett. **91**, 151106 (2007).
[19]A. N. Tait, T. Ferreira de Lima, M. A. Nahmias, B. J. Shastri, and P. R. Prucnal, "Continuous calibration of microring weights for analog optical networks," IEEE Photonics Technol. Lett. **28**, 887–890 (2016).
[20]Z. Cheng, C. Ríos, W. H. Pernice, C. David Wright, and H. Bhaskaran, "On-chip photonic synapse," Sci. Adv. **3**, e1700160 (2017).